Redox Biology 76 (2024) 103333

Contents lists available at ScienceDirect

Redox Biology

journal homepage: www.elsevier.com/locate/redox

Liver-secreted FGF21 induces sarcopenia by inhibiting satellite cell myogenesis via klotho beta in decompensated cirrhosis

Da Zhou [a,1], Yifan Shi [a,1], Donghua Zhang [a], Junbo Zuo [b,c], Chenghao Zeng [a], Gulsudum Mamtawla [a], LongChang Huang [a], Xuejin Gao [a], Li Zhang [a], Xinying Wang [a,*]

[a] Department of General Surgery, Nanjing Jinling Hospital, Affiliated Hospital of Medical School, Nanjing University, Nanjing, 210002, China
[b] Department of General Surgery, The Affiliated Jinling Hospital of Nanjing Medical University, Nanjing, 210002, China
[c] Department of General Surgery, The Affiliated People's Hospital of Jiangsu University, Zhenjiang, 210002, China

ARTICLE INFO

Keywords:
Decompensated cirrhosis
Sarcopenia
Fibroblast growth factor 21
Klotho beta
Satellite cell
PI3K/Akt

ABSTRACT

Background & aims: Sarcopenia, a prevalent condition, significantly impacts the prognosis of patients with decompensated cirrhosis (DC). Serum fibroblast growth factor 21 (FGF21) levels are significantly higher in DC patients with sarcopenia. Satellite cells (SCs) play a role in aging- and cancer-induced sarcopenia. Here, we investigated the roles of FGF21 and SCs in DC-related sarcopenia as well as the underlying mechanisms.
Methods: We developed two DC mouse models and performed in vivo and in vitro experiments. Klotho beta (KLB) knockout mice in SCs were constructed to investigate the role of KLB downstream of FGF21. In addition, biological samples were collected from patients with DC and control patients to validate the results.
Results: Muscle wasting and impaired SC myogenesis were observed in the DC mouse model and patients with DC. Elevated circulating levels of liver-derived FGF21 were observed, which were significantly negatively correlated with skeletal muscle mass/skeletal muscle index. Liver-secreted FGF21 induces SC dysfunction, contributing to sarcopenia. Mechanistically, FGF21 in the DC state exhibits enhanced interactions with KLB on SC surfaces, leading to downstream phosphatase and tensin homolog upregulation. This inhibits the protein kinase B (PI3K/Akt) pathway, hampering SC proliferation and differentiation, and blocking new myotube formation to repair atrophy. Neutralizing circulating FGF21 using neutralizing antibodies, knockdown of hepatic FGF21 by adeno-associated virus, or knockout of KLB in SCs effectively improved or reversed DC-related sarcopenia.
Conclusions: Hepatocyte-derived FGF21 mediates liver-muscle crosstalk, which impairs muscle regeneration via the inhibition of the PI3K/Akt pathway, thereby demonstrating a novel therapeutic strategy for DC-related sarcopenia.

1. Introduction

Liver cirrhosis, a chronic liver disease characterized by progressive and irreversible liver dysfunction, accounts for 2.4 % of all deaths worldwide [1]. Once liver cirrhosis progresses to the decompensated stage, the median survival time of patients is shortened to 2–4 years, and the ultimate treatment is liver transplantation (LT) [2]. In China, approximately half of the patients who undergo LT are diagnosed with decompensated cirrhosis (DC) [3]. However, these patients are prone to sarcopenia (skeletal muscle mass loss and dysfunction) before LT, with an incidence rate of 46.7 % [4], leading to increased postoperative complications, prolonged ICU stay, and reduced survival rate [5,6]. Current strategies for improving sarcopenia include nutritional supplementation, resistance exercise, blood ammonia reduction, and hormone replacement therapy; however, these strategies have exhibited limited effectiveness [7]. Therefore, it is necessary to further understand the pathophysiological mechanisms underlying DC-related sarcopenia to develop novel therapeutic strategies.

Previous studies have indicated an indirect link between the liver and skeletal muscles. Liver dysfunction during DC leads to elevated blood ammonia and estrogen levels, resulting in decreased skeletal

* Corresponding author. Department of General Surgery, Nanjing Jinling Hospital, Affiliated Hospital of Medical School, Nanjing University, 305 East Zhongshan Road, Nanjing, 210002, China.
E-mail address: wangxinying@nju.edu.cn (X. Wang).
[1] These authors have contributed equally to this work.

https://doi.org/10.1016/j.redox.2024.103333
Received 19 July 2024; Received in revised form 28 August 2024; Accepted 29 August 2024
Available online 30 August 2024

List of abbreviations

AAV	adeno-associated virus
ALT	alanine aminotransferase
AST	aspartate aminotransferase
CCL4	carbon tetrachloride
DC	decompensated cirrhosis
DDC	5-diethoxycarbonyl-1,4-dihydrocollidine
FGF15	fibroblast growth factor 15
FGF19	fibroblast growth factor 19
FGF21	fibroblast growth factor 21
FGF23	fibroblast growth factor 23
GC	gastrocnemius
KLB	klotho beta
LT	liver transplantation
MELD	Model for End-Stage Liver Disease
Myf5	myogenic factor 5
Myod	myogenic differentiation
Myog	myogenin
NC	normal control
PI3K/Akt	protein kinase B
Pax7	paired box protein 7
PTEN	phosphatase and tensin homolog
SCs	satellite cells
TA	tibialis anterior muscle

muscle protein synthesis and increased catabolism [8,9], contributing to muscle wasting. The liver is an endocrine organ that performs metabolic functions. The increased release of hepatokines in circulation, which is triggered by liver damage, may directly affect the cardiovascular system, brain, kidneys, and lungs [10–12]. However, the direct relationship between the liver and skeletal muscle loss in DC has not been elucidated thus far.

In addition to regulating protein synthesis and catabolism, muscle stem cells (termed satellite cells, SCs) are pivotal in preserving skeletal muscle mass. Positioned between the basal lamina of muscle fibers and the plasma membrane, SCs rapidly proliferate and differentiate to regenerate new muscle fibers to repair damaged myotubes following muscle injury [13]. SC dysfunction leads to age-related and cancer-induced muscle wasting, underscoring their significance in maintaining muscle mass [14,15]. In a mouse model of portosystemic shunting-induced cirrhosis, SC dysfunction contributed to muscle loss, indicating their involvement in cirrhosis-related sarcopenia [16]. Maintaining normal SC function is a promising strategy for sarcopenia treatment. However, the effects of hepatokines on SCs in DC have not yet been reported.

The fibroblast growth factor (FGF) family consists of 22 related proteins divided into seven subfamilies [17]. FGF21, belonging to the FGF19 subfamily, is primarily secreted by the liver, acting as an endocrine factor due to its lack of affinity for heparin sulfate, and plays a role in regulating glucose and lipid metabolism via the receptor FGFR1-2/klotho beta (KLB) [18]. Under healthy conditions, FGF21 does not influence skeletal muscle homeostasis [19]. FGF21 can have anti diabetic cardiomyopathy effects through the FGF21-KLB-SIRT3 axis [20], and may play a role in the treatment of stroke by reducing the activity of the NF-κB pathway and improving the PPAR-γ pathway through its actions on FGFR1 [21]. However, it may act as a causative factor or mediator of skeletal muscle atrophy in animal models of fasting [22] or mitochondrial deficiency [23]. Interestingly, serum FGF21 levels are significantly higher in liver cirrhosis patients with sarcopenia than in those without [24]. Surprisingly, the receptor for FGF21 (FGFR1) has also been detected in SCs [25]. Thus, we hypothesized that FGF21 may be involved in DC-related sarcopenia caused by SC dysfunction; however, the underlying molecular mechanism has not yet been elucidated.

The aim of this study was to investigate the roles of FGF21 and SCs in DC-related sarcopenia, and to elucidate the underlying mechanisms.

2. Materials and methods

2.1. Patients

Patients with DC who underwent LT and those with cholelithiasis (as controls) were enrolled at Jinling Hospital. Liver, rectus abdominis and blood samples were obtained from these patients. This study conformed to the ethical guidelines of the 1975 Declaration of Helsinki and was approved by the Ethics Committee of Jinling Hospital (No. 2023DZKY-118-01), written informed consent was obtained from each patient.

2.2. Animals and treatment

All experimental animals were housed in a specific pathogen-free facility under a 12-h light/dark cycle with ad libitum access to food and water. C57BL/6J mice were purchased from Gem Pharmatech (Nanjing, China).

Two animal models were used to simulate the link between the liver and skeletal muscles. Male C57BL/6J mice (aged 8–12 weeks) were randomized and received a normal diet (NC) (Dyets, AIN-93G, USA) or a diet supplemented with 0.1 % 5-diethoxycarbonyl-1,4-dihydrocollidine (DDC) (Dyets, D200309, USA) for 12 weeks, detailed formulations are provided in Table S3. For carbon tetrachloride (CCL4) (Sigma, 56-23-5, USA) administration, CCL4 was mixed with olive oil at a volume ratio of 1:4. 8–12 weeks old male C57BL/6J mice were randomly assigned to receive two intraperitoneal injections of CCl4 (5 μl/g body weight) or olive oil (5 μl/g body weight; control group) every week on Tuesday and Friday for six consecutive weeks. At the end of the experiment, the gastrocnemius (GC) muscle, tibialis anterior muscle (TA), soleus muscle, liver, kidney, heart, pancreas, and blood samples were collected after euthanization under anesthesia and stored at – 80 °C until processing.

Mice with Pax7-CreER carries the Cre recombinase gene, the expression of which is regulated by Pax7 promoter, which can target the recombinase to skeletal muscle satellite cells. Mice with KLB-specific deletions in SCs were generated by crossing mice carrying the Pax7-CreER and $KLB^{flox/flox}$ allele. $KLB^{SC/KO}$ (KLB-specific knockout in SCs) was designated as Pax7-$CreER^{+/-}$ along with $KLB^{flox/flox}$, and $KLB^{SC/WT}$ (as control) was designated as Pax7-$CreER^{-/-}$ along with $KLB^{flox/flox}$. $KLB^{SC/KO}$ mice were developed via intraperitoneal injection of tamoxifen (dissolved in corn oil, 15 mg/ml), which was administered for seven days. The Pax7-CreER mice were obtained from Prof Liwei Xie at the Institute of Microbiology (Guangdong Academy of Sciences, China), and were originally purchased from The Jackson Laboratory (Stock No.

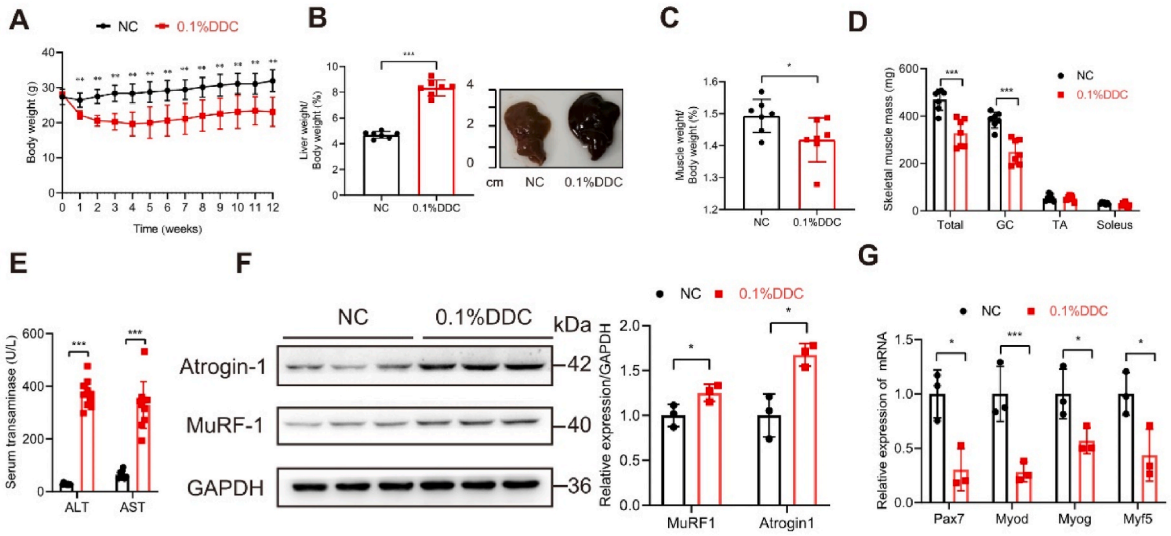

Fig. 1. Liver cirrhosis mouse model exhibited muscle atrophy and SC dysfunction
(A) Weekly changes in body weight in NC and 0.1 % DDC mice (n = 7 mice). (B) Left panel: Liver weight. Right panel: A representative image of the liver of NC and 0.1 % DDC mice at 12 weeks (n = 7 mice). (C) Ratio of skeletal muscle weight to body weight. (D) Weight of the skeletal muscle tissue in NC and 0.1 % DDC mice (n = 7 mice). (E) Measurement of blood ALT and AST levels (n = 7 mice). (F) Total protein extracts from the GC muscle of NC and 0.1 % DDC mice were immunoblotted with the indicated antibodies (n = 3 mice), and GAPDH was used as a control. (G) qRT-PCR analysis of the markers of satellite cell function in GC muscle (n = 3 mice). Data are represented as mean ± SD. Student's t-test was used to analyze statistical significance. *P < 0.05, **P < 0.01, ***P < 0.001. Abbreviations: NC, normal control; DDC, 5-diethoxycarbonyl-1,4-dihydrocollidine; ALT, alanine aminotransferase; AST, aspartate aminotransferase; GC, gastrocnemius; qRT-PCR, Quantitative reverse transcription PCR.

017763). KLB$^{flox/flox}$ mice (Stock No. T009570) were purchased from GemPharmatech (Nanjing, China).

2.3. Statistical analyses

The Student's t-test was used for comparisons between the two groups. Comparisons between multiple groups were performed using one-way ANOVA, and Bonferroni correction, Tukey's HSD, or Fisher's LSD test were used for significance level correction. Spearman's analysis was performed to evaluate correlations between the two groups. Statistical significance was set at $P < 0.05$. The aforementioned analyses were performed using GraphPad Prism software (version 8.0.2).

Power analysis: based on relevant data available in this investigation, the mean difference in serum FGF21 concentrations between the control and patients with DC was −105.3, with standard deviations of 36.1 and 34.5, respectively. Taking into account an alpha error level at two tails of 5 %, the study had 100 % power.

Additional methods are described in the Supplemental Materials and Methods.

3. Results

3.1. Mice with liver cirrhosis exhibited muscle wasting and the decreased myogenic capacity of SCs

We developed a diet-induced liver cirrhosis mouse model by administering 0.1 % DDC to mice. After 12 weeks of intervention, the body weight of the 0.1 % DDC mice was consistently lower than NC mice from the first week (Fig. 1A). At the same time, the livers of these mice were notably enlarged and accounted for approximately 8.2 % of the total body weight (Fig. 1B). Additionally, analysis of the three skeletal muscles, the GC, TA, and soleus, suggested that the proportion of skeletal muscle weight decreased, and total skeletal muscle weight was substantially reduced in 0.1 % DDC mice, with apparent atrophy of the GC (Fig. 1C–D and Fig. S1A). This was further confirmed by the body composition analysis results (Figs. S1C–D). The serum transaminase concentration was significantly higher in 0.1 % DDC mice than in NC mice (Fig. 1E). Histological staining revealed structural disorders of the liver lobulae, fibrotic cord formation, and pseudolobulae, which were confirmed by the Ishak score in 0.1 % DDC mice (Figure S1E and Figure S1F). Hence, 0.1 % DDC mice exhibited a marked decline in liver function and structure, consistent with DC. Furthermore, mean cross-sectional area (CSA) analysis of the GC muscle showed that the resulting average fiber size was significantly decreased in 0.1 % DDC mice when compared to that in NC mice (1174 μm^2 vs 2049 μm^2, Fig. S1B). The grip strength of the limbs was also markedly reduced in 0.1 % DDC mice when compared to NC mice (Fig. S1G). However, these changes were not related to food intake (Fig. S1H). Additionally, the CCL4-induced liver cirrhosis mouse model (Figs. S2A and S2D) exhibited discernible body weight loss (Fig. S2B), GC muscle mass reduction (Fig. S2B), grip strength reduction (Fig. S2C), and a significantly lower mean CSA of the GC muscle (Fig. S2E) compared to NC mice after 6 weeks of intervention.

Finally, we observed increased protein expression of the muscle atrophy-related genes encoding Atrogin-1 and MuRF-1 (Fig. 1F). The mRNA expression of paired box protein 7 (Pax7), myogenic differentiation (Myod), myogenic factor 5 (Myf5), and myogenin (Myog) was significantly decreased (Fig. 1G) in 0.1 % DDC mice compared to NC mice. Overall, sarcopenia developed in mouse models of liver cirrhosis along with impaired SC function.

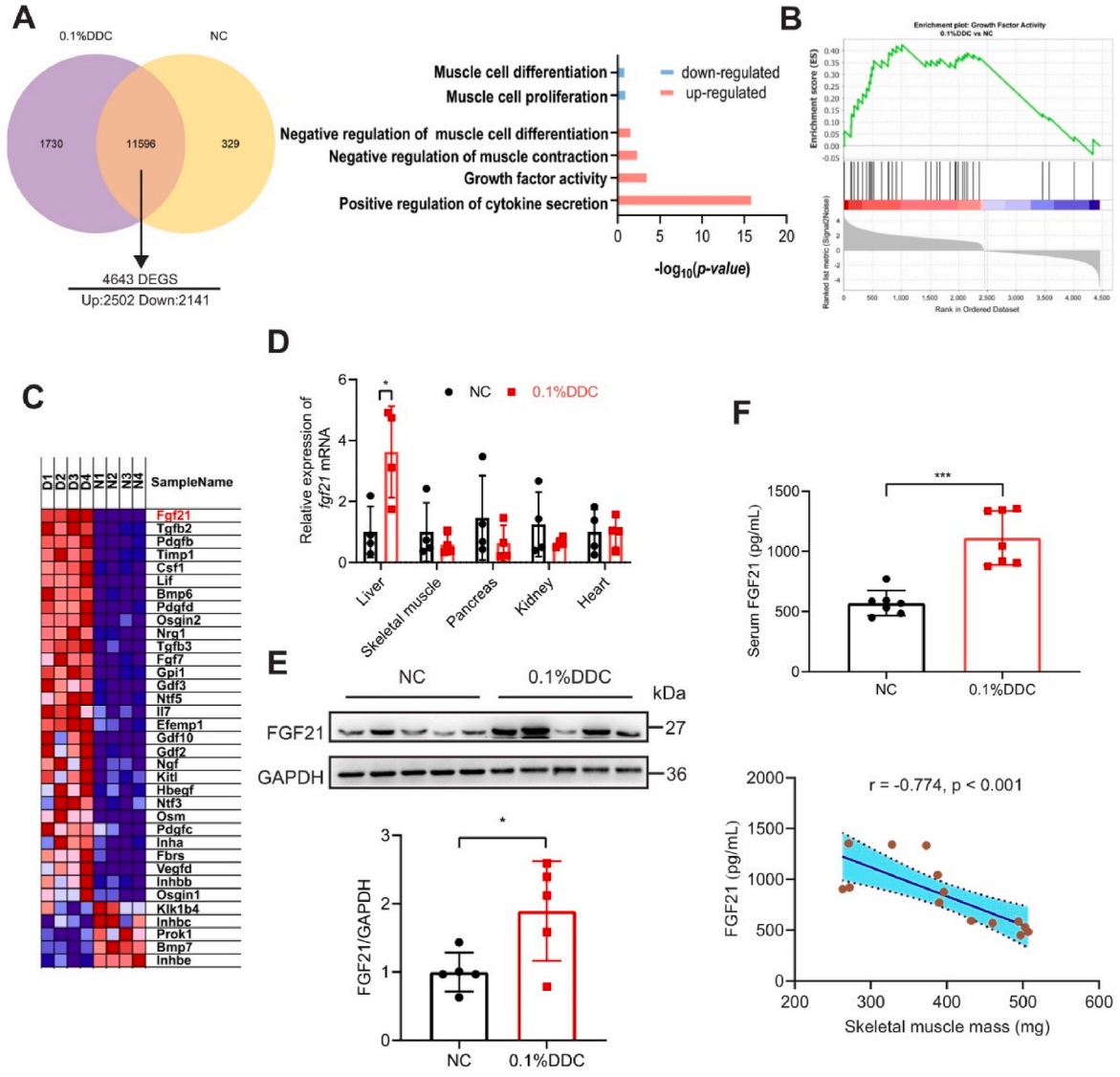

Fig. 2. Excessive FGF21 secretion by the liver is positively correlated with skeletal muscle atrophy in the liver cirrhosis mouse model
(A) Left panel: Venn diagram displaying overlapping genes between the liver tissues of 0.1 % DDC and NC mice (n = 4 per group); Right panel: GO (biological process) analysis indicating up- and downregulated genes in 0.1 % DDC and NC mice. (B) GSEA of pathways upregulated in response to growth factor activity. (C) The expression pattern of genes involved in the gene set related to growth factor activity is shown. (D) qRT-PCR analysis of Fgf21 in different organs of 0.1 % DDC and NC mice (n = 4 mice). (E) Top panel: Total protein extracts from the GC muscle of NC and 0.1 % DDC mice were immunoblotted with FGF21 antibodies (n = 5 mice), and GAPDH was used as a control. Bottom panel: Semi-quantitative analysis. (F) Top panel: Blood FGF21 measurement (n = 7 mice); Bottom panel: Spearman's correlation analysis of serum FGF21 and skeletal muscle mass. Data are represented as mean ± SD. Student's t-test was used to determine statistical significance, unless otherwise stated. *P < 0.05, **P < 0.001, ***P < 0.001. Abbreviations: NC, normal control; DDC, 5-diethoxycarbonyl-1,4-dihydrocollidine; GO, Gene ontology; GSEA, Gene Set Enrichment Analysis; GC, gastrocnemius; qRT-PCR, Quantitative reverse transcription PCR.

Table 1
Characteristics of patients received nutritional support, physical activity, and grip strength.

	Controls	Decompensated cirrhosis	P value
Received nutritional support (n, %)	3 (12.5 %)	15 (31.25 %)	0.071
5-time chair stand test (s)	9.54 (7.49–10.98)	10.51 (9.67–12.04)	0.057
Handgrip strength (kg)	32.3 (24.3–37.3)	26.1 (20.1–32.2)	0.212

3.2. Excessive secretion of FGF21 by the cirrhotic liver is positively correlated with skeletal muscle atrophy

RNA-Seq was performed to analyze the liver tissues of NC and 0.1 % DDC mice. Heat maps of gene expression in the liver indicated significant differences in the expression trends (Fig. S2F). These genes could be divided into two clusters: clusters I and II with progressively increasing and decreasing expressions, respectively. A total of 4643 differentially expressed genes (DEGs) were identified, of which 2502 were upregulated and 2141 were downregulated in 0.1 % DDC mice when compared to NC mice (Fig. 2A). Gene Ontology (GO) analysis revealed significant downregulation of muscle proliferation and differentiation in the biological processes, whereas growth factor activity and cytokine secretion were significantly upregulated in the livers of 0.1 % DDC mice (Fig. 2A). The upregulation of growth factor activity (Fig. 2B) and growth factor

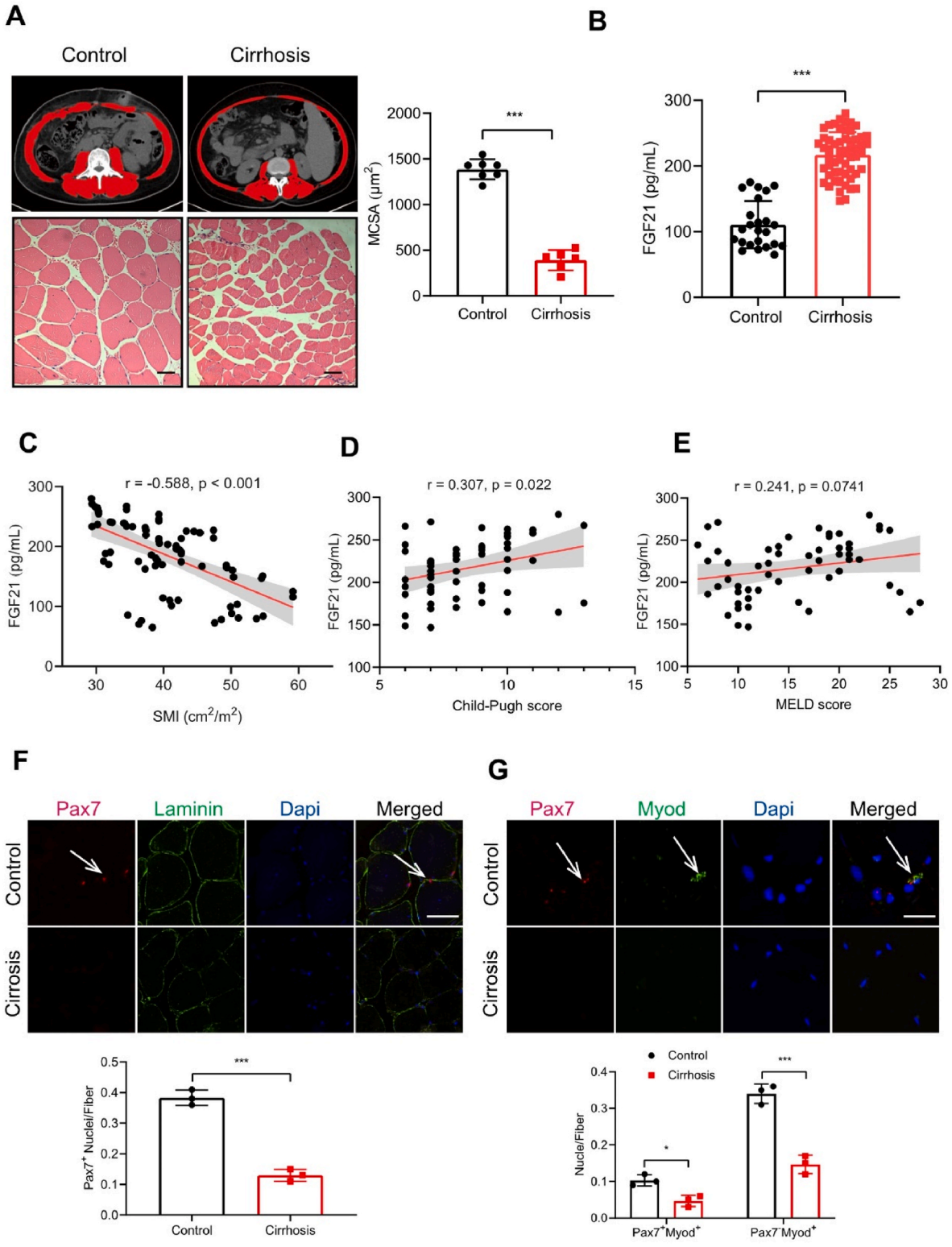

(caption on next page)

Fig. 3. Increased production of FGF21 and impaired function of muscle satellite cells in patients with decompensated cirrhosis
(A) Left panel: The representative images of skeletal muscle in L3 plane and H&E staining of rectus abdominis muscle in control patients and those with decompensated cirrhosis. Scale bars: 100 μm. Right panel: Cross-sectional areas (μm^2) of rectus abdominis muscle of control patients and those with decompensated cirrhosis (n = 7 patients in the control group; n = 6 patients in the decompensated cirrhosis group). (B) FGF21 blood levels in the control group (n = 24 patients) and the decompensated cirrhosis group (n = 48 patients). (C) Spearman's correlation analysis of serum FGF21 and SMI. (D) Spearman's correlation analysis of serum FGF21 and Child-Pugh score. (E) Spearman's correlation analysis of serum FGF21 and MELD score. (F) Upper panel: representative images of immunofluorescent staining for Pax7 (red) and laminin (green) in the rectus abdominis muscle section from control patients and those with decompensated cirrhosis. Nuclei were labeled with DAPI (blue). Scale bars: 20 μm. Lower panel: The average number of $Pax7^+$ SCs per section of rectus abdominis muscle of control patients and those with decompensated cirrhosis (n = 3 patients). (G) Upper panel: representative images of immunofluorescent staining for Pax7 (red) and MyoD (green) in the rectus abdominis muscle section from control patients and those with decompensated cirrhosis. Nuclei were labeled with DAPI (blue). Scale bars: 20 μm. Lower panel: The average number of $Pax7^+MyoD^+$ and $Pax7^-MyoD^+$ SCs per section of rectus abdominis muscle of control patients and those with decompensated cirrhosis (n = 3 patients). The data are shown as mean ± SD. Student's t-test was used to determine statistical significance unless otherwise stated. *P < 0.05, **P < 0.01, ***P < 0.001. Abbreviations: H&E, hematoxylin and eosin; qRT-PCR, Quantitative reverse transcription PCR; SMI, skeletal muscle index; MELD, Model for end-stage liver disease. (For interpretation of the references to colour in this figure legend, the reader is referred to the Web version of this article.)

receptor binding-related (Fig. S2G) biological functions in the 0.1 % DDC group was also confirmed by Gene Set Enrichment Analysis (GSEA), with FGF21 being the first upregulated gene (Fig. 2C). qRT-PCR indicated that FGF21 mRNA levels were significantly increased in the livers of 0.1 % DDC mice (Fig. 2D), which was further confirmed by western blotting and immunohistochemistry (Fig. 2E and S2H). Simultaneously, serological FGF21 concentrations increased in 0.1 % DDC mice (Fig. 2F) and were negatively correlated with skeletal muscle mass ($r = -0.774$, $P < 0.001$, Fig. 2F). Interestingly, we observed the same phenotype in CCL4 mice with increased hepatic FGF21 mRNA (Fig. S2J) and blood FGF21 levels (Fig. S2K), which were negatively correlated with muscle weight (Fig. S2L). No differences in the mRNA levels of endoplasmic reticulum (ER) stress marker (ATF4, Fig. S2I) were noted in the liver. Hence, excessive FGF21 production and release into the blood during cirrhosis may be associated with skeletal muscle wasting.

3.3. Increased production of FGF21 and decreased SC function in patients with DC

In a cohort of patients withDC who underwent LT (48 serum samples and 26 skeletal muscle and liver tissues) and patients with hepatic hemangioma who underwent hepatectomy (24 serum samples and 10 skeletal muscle and liver tissues), we observed that patients withDC exhibited a higher rate of nutritional support, a longer 5-time chair stand test, and a lower grip strength; however, the differences were not statistically significant (Table 1). We measured the skeletal muscle area at the third lumbar level, performed hematoxylin & eosin (H&E) staining of the rectus abdominis muscle and quantitative analysis of the mean CSA of muscle fibers. In patients with DC when compared to those in the control group, the results revealed increased skeletal muscle loss in abdominal CT images, the rectus abdominis is atrophied in cross-section and partially converted into a triangular shape in HE staining, and a significantly reduced mean CSA (390 μm^2 vs. 1386 μm^2, Fig. 3A). Immunohistochemistry and qRT-PCR confirmed that FGF21 protein and mRNA levels were markedly increased in cirrhotic livers (Figs. S4A–B). Consistent with the mouse models, serum FGF21 was also significantly elevated in patients with DC (Fig. 3B) and inversely correlated with skeletal muscle index (SMI) ($r = -0.588$, $P < 0.001$; Fig. 3C). In addition, blood FGF21 concentrations were moderately positively correlated with the Child-Pugh score ($r = 0.307$, $P = 0.022$; Fig. 3D) but not with the Model for End-Stage Liver Disease (MELD) score (Fig. 3E). FGF15/19 and 23 also belong to the FGF19 subfamily and share functional similarities with FGF21. We found that there was no significant difference in FGF19 (Fig. S3A) and FGF23 (Fig. S3B) mRNA expression between liver and skeletal muscle tissues from controls and patients with DC. Although the liver serum FGF19 (Fig. S3C) and FGF23 (Fig. S3D) concentrations were significantly higher in patients with DC, there was no significant correlation between serum FGF19/23 and skeletal muscle index (Figs. S3C–S3D). Consistent with the patient results, FGF15/23 mRNA expression in the liver and skeletal muscle did not change significantly after 12 weeks of 0.1 % DDC feeding in the mouse model (Figs. S3E–F). Serum FGF15/23 in 0.1 % DDC mice was higher than that in NC mice; however, there was still no marked correlation between FGF15/23 and skeletal muscle mass (Figs. S3G–H). These results suggest that FGF15/19 and FGF23 are not involved in the effects of the liver on skeletal muscle wasting in DC.

Here, we visually examined the number of SC and the status of SC proliferation and differentiation using immunofluorescence staining. The number of Pax7-positive myofibers, Pax7 Myod double-positive, and Myod single-positive muscle fibers was significantly reduced in patients with DC (Fig. 3F and G). Furthermore, western blotting and quantitative analysis revealed impaired myogenic capacity of SCs in patients with DC (Figs. S4C and S4D), which was indicated by low Pax7, Myod, and myosin heavy chain expression. Hence, DC induces increased FGF21 production in patients, leading to elevated circulating levels upon release into the bloodstream. This may induce SC dysfunction, leading to skeletal muscle atrophy.

3.4. Liver-produced FGF21 affects skeletal muscle mass and SC via blood circulation

Since the blood FGF21 levels were elevated and significantly negatively correlated with skeletal muscle mass/SMI in both liver cirrhosis mouse models and human patients, we can assume that it may be associated with skeletal muscle loss. We aimed to reduce in vivo circulation of FGF21 to modulate the corresponding signaling pathway.

NC and 0.1 % DDC mice received FGF21 neutralizing antibody (100 μg/kg) or IgG starting at 12 weeks of intervention once a day for two consecutive weeks (Fig. 4A). Neutralization of circulating FGF21 reduced the blood FGF21 concentration in 0.1 % DDC mice to levels similar to those in the NC mice (Fig. S5A). Administration of anti-FGF21 prevented continued body weight loss in 0.1 % DDC mice (Fig. S5C). In fact, the 0.1 % DDC mice exhibited a significant increase in global skeletal muscle mass after treatment; however, it was still lower than that in the NC mice (Figs. S5D and S5E). This was associated with a significant improvement in GC muscle weight (Fig. 4B, Figs. S5F and S5G). Interestingly, blood FGF21 concentrations were negatively correlated with skeletal muscle mass at the end of treatment ($r = -0.701$, $P = 0.003$; Fig. S5B). After treatment, H&E staining of the GC muscle indicated that the morphology of the fibers in 0.1 % DDC mice was restored to normal (Fig. S5H), and the muscle fiber area frequency distribution curve shifted to the right (Fig. 4C). Surprisingly, both grip

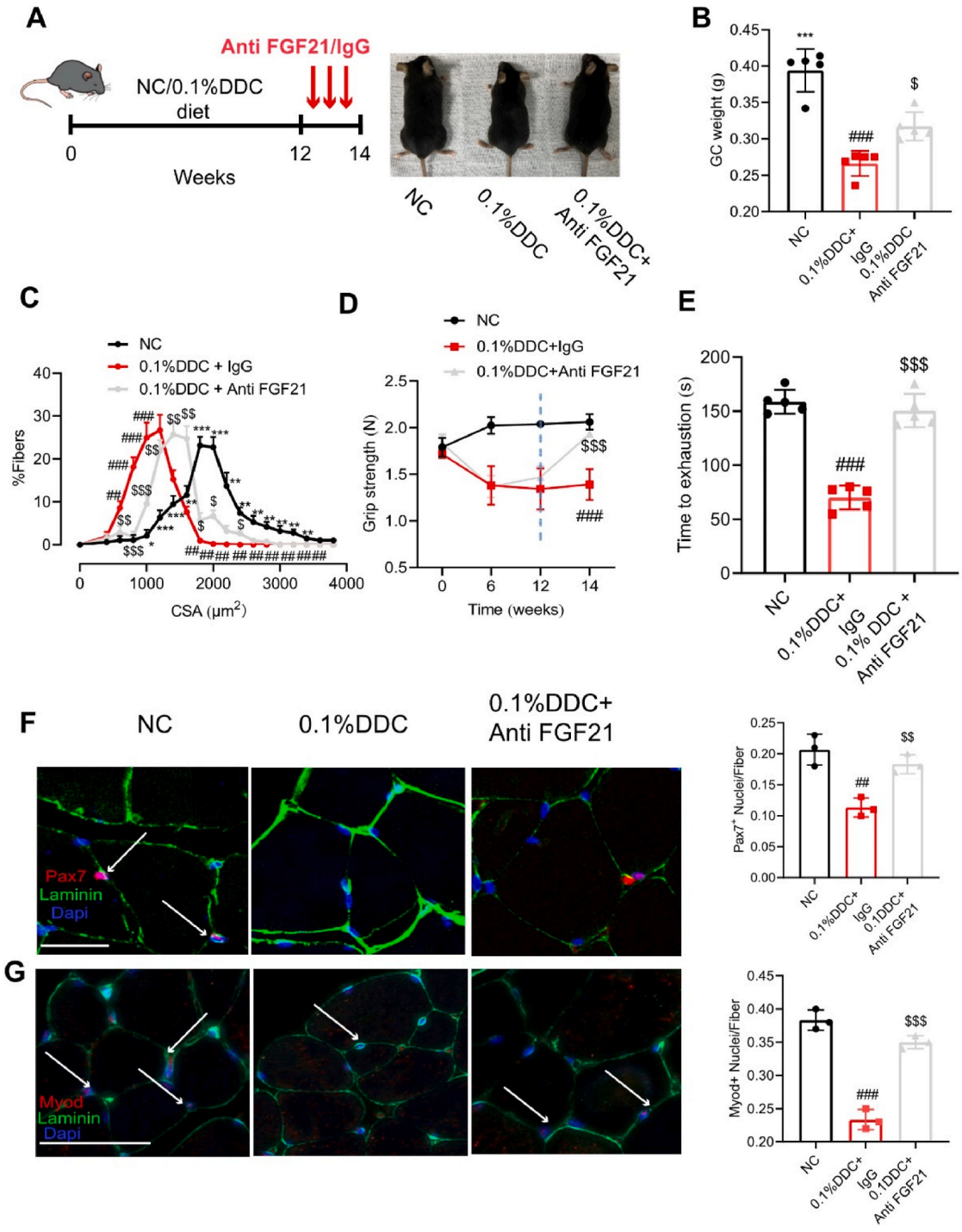

Fig. 4. Inhibition of serum FGF21 prevents muscle wasting and improves SC function in experimental liver cirrhosis model
(A) Left panel: experimental scheme of the treatment of NC and 0.1 % DDC mice via intraperitoneal injections of IgG or 100 μg/kg of FGF21 neutralizing antibody administered every day, starting at 12 weeks of age for 2 weeks. Right panel: Representative image of 14-week-old mouse model; body size of NC, 0.1 % DDC, and 0.1 % DDC + Anti-FGF21 mice. (B) Weight of GC muscles of NC, 0.1 % DDC, and 0.1 % DDC + Anti-FGF21 mice (n = 5 mice). (C) Frequency distribution plots of cross-sectional areas of the GC muscle group of the NC, 0.1 % DDC, and 0.1 % DDC + Anti-FGF21 mice (n = 3 mice). (D) Trends in grip strength in NC, 0.1 % DDC, and 0.1 % DDC + Anti-FGF21 mice (n = 5 mice). (E) Time to exhaustion in NC, 0.1 % DDC, and 0.1 % DDC + Anti-FGF21 mice (n = 5 mice). (F) Left panel: Representative images of immunofluorescent staining for Pax7 (red) and laminin (green) in GC muscle sections of NC, 0.1 % DDC, and 0.1 % DDC + anti-FGF21 mice. The nuclei were labeled using DAPI (blue). Scale bars: 25 μm; Right panel: The average number of Pax7-positive SCs ($Pax7^{+}$) per GC section of three groups of mice (n = 3 mice). (G) Left panel: Representative images of immunofluorescent staining for Myod (red) and laminin (green) in GC muscle sections of NC, 0.1 % DDC, and 0.1 % DDC + anti-FGF21 mice. The nuclei were labeled using DAPI (blue). Scale bars: 10 μm. Right panel: The average number of Myod-positive SCs (Myod+) per GC section of three groups of mice (n = 3 mice). Data are shown as mean ± SD. The one-way ANOVA was used to analyze statistical significance. * when NC vs. 0.1 % DDC + anti-FGF21, $ when 0.1 % DDC vs. 0.1 % DDC + anti-FGF21, # when NC vs. 0.1 % DDC. $^{*,\$,\#}P < 0.05$, $^{**,\$\$}P < 0.01$, $^{***,\$\$\$,\#\#\#}P < 0.001$. Abbreviations: NC: normal control; DDC, 5-diethoxycarbonyl-1,4-dihydrocollidine; GC, gastrocnemius; qRT-PCR, quantitative reverse transcription PCR. (For interpretation of the references to colour in this figure legend, the reader is referred to the Web version of this article.)

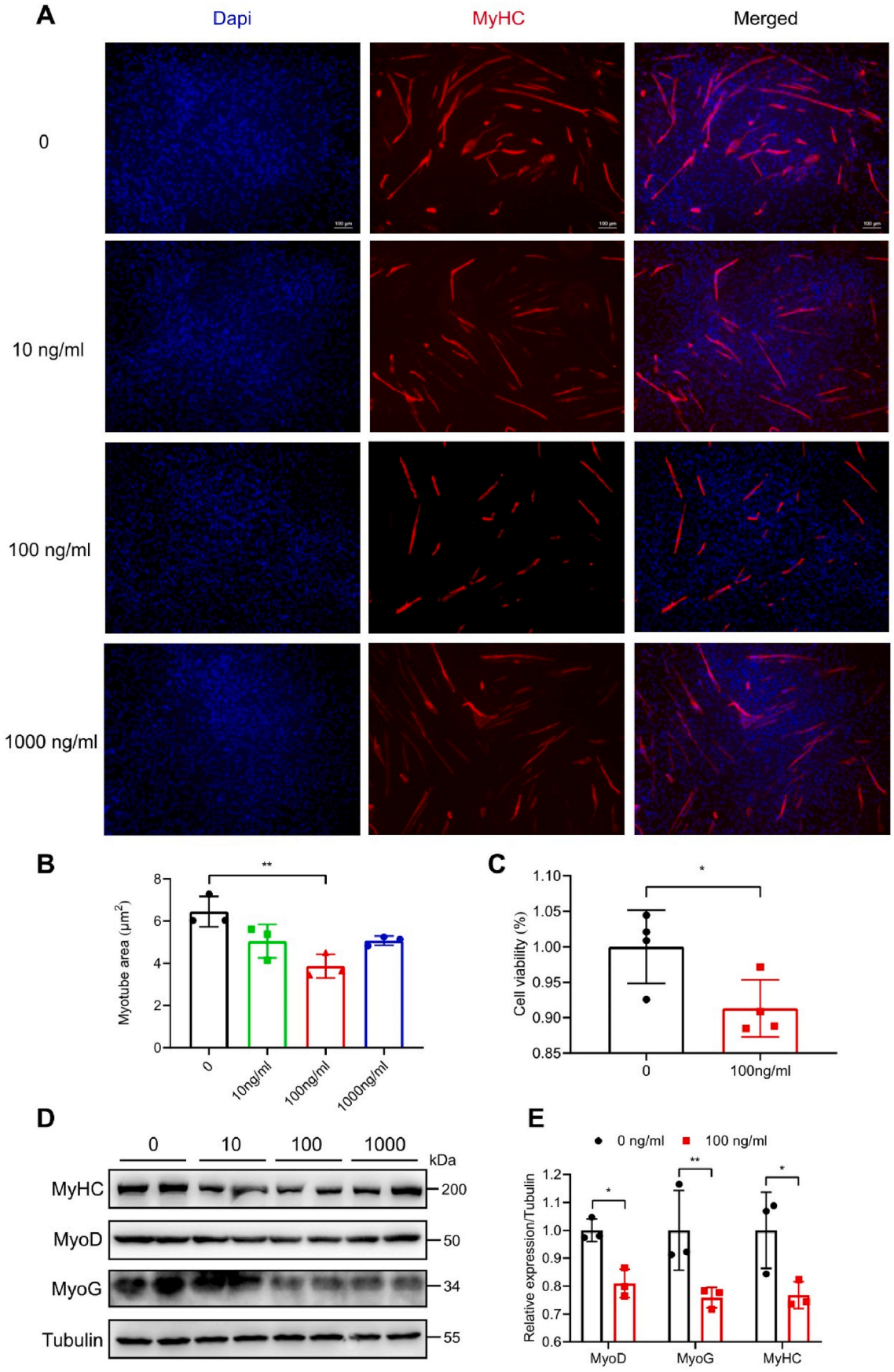

(caption on next page)

Fig. 5. Recombinant FGF21 protein inhibited myoblast differentiation in vitro
(A) Representative images of immunofluorescence staining for MyHC in C2C12 myoblasts during differentiation after being treated with different concentrations of recombinant FGF21, respectively. Nuclei were labeled with DAPI (blue). Scale bars: 100 μm. (B) Area of myotubes after treatment with different concentrations of recombinant FGF21 (n = 3 myotube). (C) Effects of recombinant FGF21 on C2C12 activity and proliferation (n = 4 myotube). (D) Total protein extracts from myotubes were immunoblotted with the indicated antibodies (n = 3 myotube), and tubulin was used as a control. (F) Quantitative analysis of Western blot (n = 3 myotube) results. The data are shown as mean ± SD. One-way ANOVA and Student's t-test were used to determine statistical significance. *P < 0.05, **P < 0.01. (For interpretation of the references to colour in this figure legend, the reader is referred to the Web version of this article.)

strength and endurance in anti-FGF21-treated 0.1 % DDC mice were restored to levels similar to those in NC mice (Fig. 4D and E). Furthermore, the mRNA levels of the muscular atrophy-related genes were restored to normal levels after treatment (Fig. S5I).

Next, we evaluated the effect of anti-FGF21 treatment on SC function. First, the number of SCs was assessed by quantitative analysis of Pax7-positive immunofluorescence staining results. The number of $Pax7^{+}$-SCs increased remarkably in anti-FGF21-treated 0.1 % DDC mice (Fig. 4F). Second, positive immunofluorescence staining for $MyoD^{+}$ revealed the initiation of differentiation in SCs, and the number of $MyoD^{+}$ cells was significantly increased after neutralization with the FGF21 antibody (Fig. 4G). Finally, the mRNA levels of Pax7 and Myod significantly increased in 0.1 % DDC mice after intervention (Fig. 4SJ), confirming the restoration of SC function. Hence, circulating FGF21 negatively affects SCs, leading to skeletal muscle atrophy.

3.5. Recombinant FGF21 protein inhibits myoblast differentiation in vitro

To further elucidate the effect of FGF21 on myoblast differentiation, recombinant FGF21 protein was added to the culture medium. We set three concentration gradients (10, 100, and 1000 ng/ml) to explore the optimal dose for administration. C2C12 myoblasts were then incubated with different concentrations of recombinant FGF21 protein. Immunofluorescence staining of myosin heavy chain (MyHC) demonstrated that C2C12 myoblasts incubated with 100 ng/ml of recombinant FGF21 had the lowest number of myotubes (Fig. 5A). Furthermore, measurement of the myotube area indicated that the most significant skeletal muscle atrophy was observed with 100 ng/ml of FGF21 recombinant protein (Fig. 5B). Cell viability was detected using the CCK-8 assay 48 h after administration; 100 ng/ml of recombinant protein reduced myoblast proliferation (Fig. 5C). Consistently, 100 ng/ml of FGF21 recombinant protein also effectively suppressed the protein expression levels of myogenesis-related genes, including Myod, Myog, and MyHC, in C2C12 myoblasts during differentiation (Fig. 5D and E). Hence, high concentrations of FGF21 lead to myotube atrophy and restrict myoblast differentiation, which are detrimental to skeletal muscle growth.

3.6. Skeletal muscle atrophy and SC myogenic function were improved after liver FGF21 knockdown

We constructed adeno-associated virus (AAV) shFGF21 to knock down liver FGF21 in NC and 0.1 % DDC mice, and employed AAV scramble shRNA as a negative control (Fig. 6A). We evaluated whether AAV shFGF21 exerted a silencing effect in vivo. Tail vein injection of AAV shFGF21 for 4 weeks reduced the expression of FGF21 in the liver (Figs. S6A and S6B) and serum (Fig. S6C), indicating highly efficient liver knockdown.

The efficiency of the knockdown was confirmed by determining the liver and serum FGF21 concentrations in 0.1 % DDC mice (Fig. 6B). The body weights of 0.1 % DDC mice increased significantly, whereas AAV injection had a negligible effect on NC mice (Fig. S6D). Furthermore, FGF21 knockdown in 0.1 % DDC mice resulted in the significant enhancement of muscle force and endurance (Fig. 6C and D). Importantly, the GC and TA muscles in 0.1 % DDC mice were greatly improved after shFGF21 treatment and were found to be similar to those in NC mice (Fig. 6E and S6E). Furthermore, serum transaminase did not rise after FGF21 knockdown in liver, suggesting that FGF21 knockdown of liver will not aggravate liver injury (Fig. S6F). Quantification of GC muscle H&E staining (Fig. 6F) revealed a notable shift to the right in the muscle area curve of 0.1 % DDC mice after FGF21 knockdown, which was accompanied by a remarkable increase in large muscle fiber size ($>2000\ \mu m^2$, Fig. 6G). The average CSA was elevated to a level comparable to that of the NC group (Fig. 6G). Hence, muscle atrophy in 0.1 % DDC mice was attenuated.

To examine whether the decreased proliferation and differentiation ability of SCs in sarcopenia could be reversed by shFGF21 treatment, we performed immunofluorescence staining and qRT-PCR in skeletal muscle. The number of Pax7-positive, Myod-positive (indicating proliferation), Pax7-negative, and Myod-positive (indicating differentiation) cells was notably increased, and the mRNA levels of Pax7 and Myod were markedly increased in 0.1 % DDC mice after FGF21 knockdown (Fig. 6H and I). Fiber-type analysis revealed that shFGF21 treatment promoted an increase in the mean CSA of oxidative slow-twitch fibers (type I, Fig. S6H), oxidative fast-twitch fibers (type IIa, Fig. S6I), and glycolytic fast-twitch fibers (type IIb, Fig. S6J), which also reflected the improvement in SC function (Fig. S6G).

3.7. Increased PI3K/AKT signaling in the muscles of 0.1 % DDC mice following FGF21 inhibition

To identify the downstream signaling pathways influenced by FGF21 inhibition in cirrhotic mouse muscles, we performed a transcriptomic analysis comparing scrambled shRNA-treated and shFGF21-treated GC muscles in 0.1 % DDC mice. The gene heatmap and principle component analysis plot revealed significant differences in gene expression between the two groups (Fig. 7A). Compared with scrambled shRNA-treated control mice, 705 DEGs were noted in shFGF21-treated mice, among which the expressions of 306 were upregulated and 397 were downregulated (Fig. 7B). GO analysis (biological process) identified genes that were primarily involved in the regulation of skeletal muscle development and muscle cell homeostasis. Downregulated DEGs were involved in the regulation of mitochondrial depolarization, positive regulation of collagen biosynthetic processes, I-kappaB phosphorylation, and lipid biosynthetic processes, whereas upregulated genes were mainly involved in muscle cell development, regulation of stem cell division, positive regulation of stem cell differentiation, and muscle cell cellular homeostasis (Fig. 7C). GSEA revealed that mitochondrial functions, such as oxidative phosphorylation and mitochondrial ATP synthesis, were also significantly improved after liver FGF21 knockdown (Fig. S7A). ShFGF21 treatment in 0.1 % DDC mice led to increased SDH activity in the mitochondria of muscle cells, as reflected by SDH staining (Figs. S7B and S7C). The PI3K-Akt signaling pathway is among the top KEGG signaling pathways upregulated after shFGF21 treatment of 0.1 % DDC mice (Fig. 7D). Previous studies have reported that the PI3K/Akt

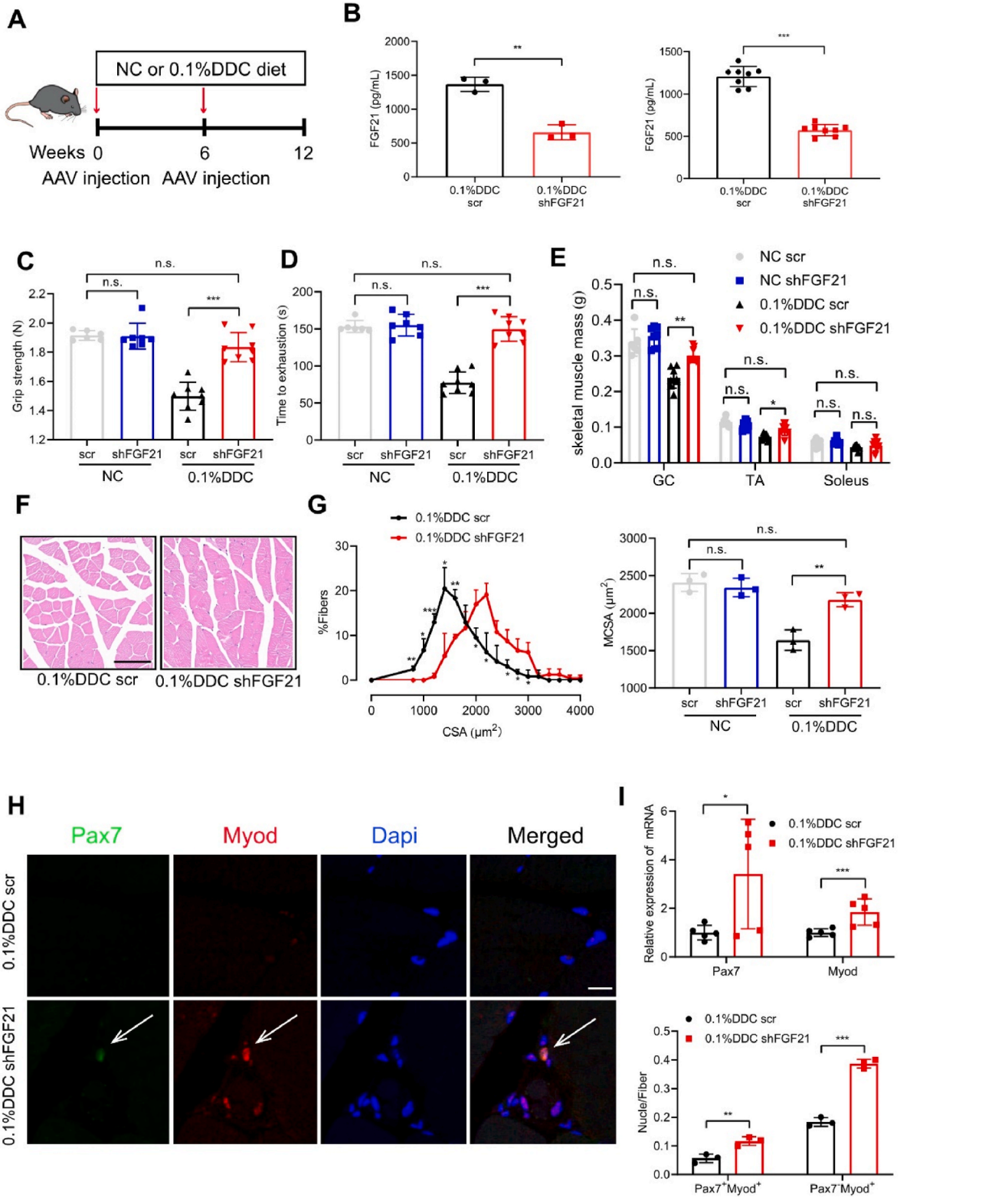

(caption on next page)

Fig. 6. Liver-specific downregulation of FGF21 protects from cirrhosis-induced skeletal muscle loss and SC dysfunction
(A) Schematic illustration of the experimental design: mice were fed a normal diet or 0.1 % DDC-supplemented diet for 12 weeks and injected with AAV-shFGF21 or AAV-scr via the tail vein before feeding and at week six after feeding. (B) Left panel: liver FGF21 levels in 0.1 % DDC mice injected with AAV-shFGF21 or AAV-scr (n = 3 mice). Right panel: blood FGF21 levels in 0.1 % DDC mice injected with AAV-shFGF21 or AAV-scr (n = 8 mice). (C, D) The grip strength and endurance of NC and 0.1 % DDC mice injected with AAV-shFGF21 or AAV-scr (n = 8 mice). (E) The weights of GC muscle, TA muscle, and soleus muscle of NC and 0.1 % DDC mice injected with AAV-shFGF21 or AAV-scr (n = 8 mice). (F) Representative H&E staining images of GC muscle derived from 0.1 % DDC mice injected with AAV-shFGF21 or AAV-scr. Scale bars: 100 μm. (G) Left panel: Frequency distribution curves of cross-sectional areas of muscles of 0.1 % DDC mice injected with AAV-shFGF21 or AAV-scr (n = 3 mice). Right panel: Mean cross-sectional area of GC muscle derived from NC and 0.1 % DDC mice (n = 3 mice). (H) Representative Pax7 and Myod immunofluorescence staining images of GC muscle of 0.1 % DDC mice injected with AAV-shFGF21 or AAV-scr. Nuclei were labeled with DAPI (blue). Scale bars: 100 μm. (I) Top panel: Percentage of Pax7-and Myod-double positive ($Pax7^{+}Myod^{+}$) muscle fibers and Pax7-negative and Myod-positive ($Pax7^{-}Myod^{+}$) muscle fibers in 0.1 % DDC mice injected with AAV-shFGF21 or AAV-scr (n = 3 mice); Bottom panel: The mRNA levels of Pax7 and Myod in 0.1 % DDC mice injected with AAV-shFGF21 or AAV-scr (n = 5 mice). Data are shown as mean ± SD. One-way ANOVA and Student's t-test were used to determine statistical significance. *P < 0.05, **P < 0.01, **P < 0.001. Abbreviations: DDC, 5-diethoxycarbonyl-1,4-dihydrocollidine; GC, gastrocnemius; TA, anterior tibialis; scr, scramble; AAV, Adeno-associated virus. (For interpretation of the references to colour in this figure legend, the reader is referred to the Web version of this article.)

pathway plays a fundamental role in regulating the proliferation and differentiation of SCs. Western blotting confirmed that PI3K/Akt pathway protein expression was increased in skeletal muscle after liver FGF21 knockdown (Fig. 7E). Importantly, PI3K/Akt protein expression was significantly reduced in the skeletal muscle of DC patients compared to that in control patients. Similar results were observed in 0.1 % DDC mouse muscles (Fig. S7D).

To further elucidate whether FGF21 regulates SC function via the PI3K/Akt signaling pathway, a PI3K inhibitor was locally injected into the GC muscle of 0.1 % DDC mice every other day for 2 weeks after AAV intervention (Fig. 7G). The GC muscle weight (Fig. 7H) and grip strength (Fig. 7I) were significantly reduced after PI3K inhibition, and body weight was similar between the two groups (Fig. S7E). H&E staining of the GC muscle (Fig. 7J) revealed that the improvement in the average CSA induced by FGF21 knockdown was reduced after PI3K inhibition (Fig. 7K). Similarly, Western blot analysis suggested that the protein expression of *p*-Akt (Fig. 7L), MyoD, and Pax7 decreased markedly after PI3K inhibition (Fig. 7M). Collectively, these results suggest that FGF21 impairs SC proliferation and differentiation by inhibiting the PI3K/Akt pathway.

3.8. DC-induced sarcopenia requires KLB

First, we studied the impact of FGFR1-4/KLB in skeletal muscle. The qRT-PCR and Western blot results showed no differences, with the exception of KLB expression, between NC and 0.1 % DDC mice at the mRNA level (Fig. 8A and Figs. S8A–S8B). The immunofluorescence results suggested that KLB could co-stain with Pax7 but not Desmin (Fig. 8B). These data indicate that skeletal muscle tissue may be a direct target of FGF21. Specifically, it may directly affect SCs. To determine the role of KLB in muscle wasting, we generated SC-specific KLB knockout ($KLB^{SC/KO}$) mice and developed DC models (Fig. 8C). KLB protein expression was remarkably reduced in the skeletal muscles of $KLB^{SC/KO}$ mice (Fig. 8D). $KLB^{SC/KO}$ mice had higher body weights (Fig. 8E) with preservation of the skeletal muscle mass (Fig. 8F and Fig. S9A) and grip strength (Fig. 8G). H&E staining of the GC muscle (Fig. 8H) revealed that $KLB^{SC/KO}$ mice could maintain normal morphology, and the mean CSA was remarkably high (Fig. S9B). More importantly, KLB knockout in SCs significantly enhanced their myogenic capacity, as indicated by the increased protein expression of Pax7 and Myod in $KLB^{SC/KO}$ mice (Fig. 8I).

We examined Phosphatase and Tensin Homolog (PTEN) expression under different conditions to determine the specific cause of the FGF21-mediated decrease in PI3K pathway activity. PTEN expression significantly increased in the skeletal muscles of 0.1 % DDC mice (Fig. 8J) and patients with DC (Fig. 8K). Interestingly, hepatic FGF21 knockdown did not affect PTEN expression in the skeletal muscles (Fig. S9C), suggesting that PTEN may be associated with KLB activation. This was confirmed by western blotting, which indicated that PTEN expression was significantly reduced after KLB knockout in SCs (Fig. 8L) and was accompanied by the upregulation of *p*-Akt expression (Fig. 8M). Taken together, these data indicate that FGF21-mediated KLB activation leads to PTEN upregulation and inhibition of the PI3K/Akt signaling pathway.

4. Discussion

Cytokines secreted by the liver regulate skeletal muscle development, growth, and mass. During liver dysfunction, cytokine function is dysregulated, leading to skeletal muscle loss and sarcopenia. Previous studies have found that insufficient nutritional intake, physical inactivity, and ascites may be associated with sarcopenia in liver cirrhosis [26]. Here, we elucidated the effect of the hepatokine FGF21 on skeletal muscle during DC. Abnormal elevation of hepatocyte-derived FGF21 aggravates the deregulation of the PI3K/Akt pathway via KLB in SCs and accelerates the development of sarcopenia. A reduction in elevated FGF21 or KLB levels not only improved the myogenic function of SCs, but also alleviated sarcopenia in the DC model. Thus, we identified a novel direct liver-muscle crosstalk pathway in the context of DC and provided evidence for its use as a potential therapeutic target for sarcopenia.

To the best of our knowledge, this is the first study to systematically evaluate the phenotype of sarcopenia in a preclinical DC model and show that FGF21 impairs SC proliferation and differentiation, thereby attenuating skeletal muscle growth. Whether FGF21 is beneficial or detrimental to skeletal muscle remains controversial, as its effects can vary based on the source and pathophysiology. In a fasting mouse model, excessive FGF21 production in the skeletal muscle led to muscle atrophy via enhanced mitophagy in a Bnip3-dependent manner and reduced the protein synthesis rate [22]. However, in a catheterized mouse model of critical illness induced by surgery and sepsis, FGF21 knockout aggravated muscle loss, which may be related to the accumulation of cellular ER stress [27]. Sarcopenia is associated with elevated serum FGF21 levels in patients with cirrhosis, and FGF21 is negatively correlated with grip strength, as shown by cluster network analysis [24]. FGF21 is a 210-amino acid secreted protein, which is produced by the liver and secreted into the blood, ultimately reaching the muscle cells [28]. In our study, both theDC mouse model and patient data further support the hypothesis that elevated serum FGF21 is facilitated by the liver and is significantly negatively correlated with skeletal muscle mass/SMI. More importantly, the harmful effects of FGF21 on skeletal muscle disappeared when the FGF21 blood concentration and expression in the liver returned to normal, suggesting that the liver

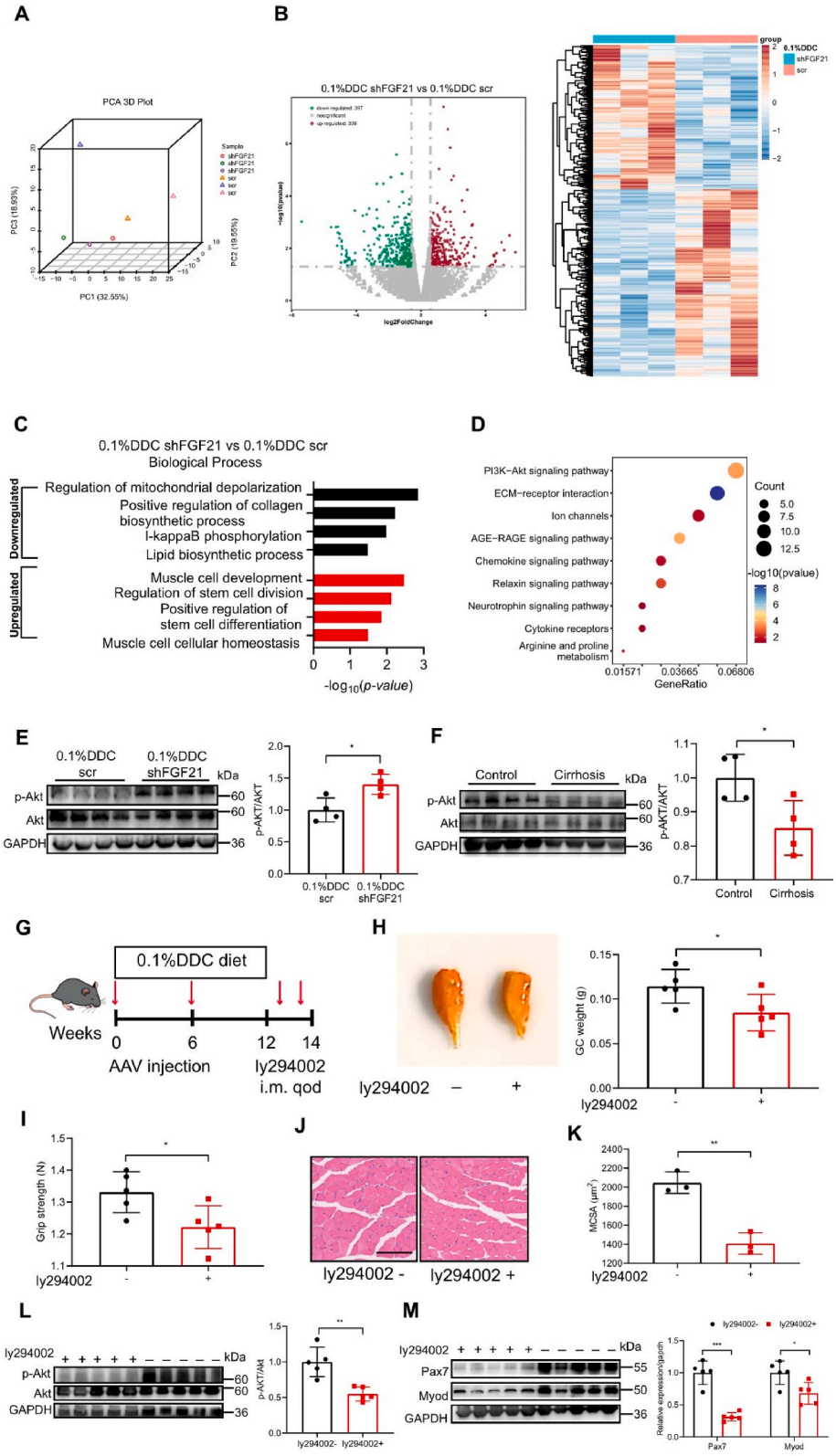

(caption on next page)

Fig. 7. Liver FGF21 inhibition alters PI3K/Akt signaling pathway to improve SC function
(A) 3D principal component analysis of gene expression in 0.1 % DDC mice liver treated with AAV shFGF21 or AAV scramble (n = 3 mice). (B) Left panel: Volcano plot of the gene expression in (A). Right panel: Heatmap of differentially expressed genes identified in the liver of 0.1 % DDC mice treated with AAV shFGF21 or AAV scr. (C) GO (biological process) analysis of downregulated (black) and upregulated (red) processes. (D) Scatter plots for KEGG pathway analysis of differentially expressed genes. (E–F) Western blot of *p*-Akt in the muscle of 0.1 % DDC mice, and quantitative analysis of the results after shFGF21 or scr treatment (n = 4 mice) and in control or muscles of cirrhosis patients (n = 4 patients). (G) Experimental scheme: 0.1 % DDC mice received AAV shFGF21 treatment twice followed by local skeletal muscle injection of PBS or PI3K inhibitor for two weeks. (H) Left panel: Representative images of GC muscle in 0.1 % DDC mice injected with AAV shFGF21 followed by LY294002 or PBS intervention. Right panel: GC muscle weight in 0.1 % DDC mice injected with AAV shFGF21 followed by LY294002 or PBS intervention (n = 5 mice). (I) Grip strength in 0.1 % DDC mice injected with AAV shFGF21 followed by LY294002 or PBS intervention (n = 5 mice). (J) Representative H&E staining images of GC muscles from 0.1 % DDC mice injected with AAV shFGF21 followed by LY294002 or PBS intervention. Scale bars: 100 μm. (K) The average cross-sectional area of GC muscle in (J). (L–M) Left panel: Total protein extracts from GC muscle were immunoblotted with the indicated antibodies (n = 5 myotube), and GAPDH was used as a control. Right panel: the quantitative analysis of Western blot (n = 5 mice). Data are shown as mean ± SD. Student's t-test was used to determine statistical significance. *P < 0.05, **P < 0.01, ***P < 0.001. Abbreviations: DDC, 5-diethoxycarbonyl-1,4-dihydrocollidine; GC, gastrocnemius; GO, Gene Ontology; H&E, hematoxylin and eosin; AAV, Adeno-associated virus. (For interpretation of the references to colour in this figure legend, the reader is referred to the Web version of this article.)

directly acts on skeletal muscle by secreting FGF21. ER stress can induce the secretion of FGF21; however, ATF4 (an ER stress marker, Fig. S2I) expression in our mouse model remained unchanged. Hence, alternative pathways may be involved in activating FGF21, warranting further clarification in future studies.

We also evaluated the effects of hepatocytes on SCs during DC. SCs are adult stem cells that were discovered by Mauro in 1961 [29]. SCs are usually quiescent in their physiological state and can be divided into two subsets during muscle atrophy [30]. One subset can replenish the quiescent SC (QSC) pool, whereas the other subsequently proliferates and differentiates into new muscle fibers [31]. Pax7 is a transcription factor in SCs that plays a regulatory role in the occurrence, survival, maintenance of resting state, and proliferation of SCs [32]. Myogenic regulatory factors, such as Myod, Myf5, and Myog, facilitate cell proliferation and differentiation, and the upregulation of Myod is required for myogenesis [33,34]. An impaired SC pool and dysfunction of SC proliferation and differentiation can delay skeletal muscle repair, leading to sarcopenia. Internal factors, such as aging, oxidative stress, and DNA damage [35], and external factors, such as inflammation, cytokines, and metabolites [36], can also impair SC function. SC activation, proliferation, and differentiation are regulated by a variety of pathways, such as p38/MAPK [37], ERK/MAPK [25], and JAK/STAT3 [38], among which PI3K/Akt is the regulatory center of SC activation through mTOR activation and inhibition of FOXO in QSCs. PI3K increases mitochondrial activity in a state of mobilization before SC activation to provide sufficient energy for activation [39,40]. Here, an improvement in PI3K pathway activity was accompanied by an increase in mitochondrial activity, as indicated by the enhanced SDH levels (Fig. S7C). The PI3K/Akt signaling pathway regulates myogenesis via various pathways. Akt activation can mitigate the inhibitory effect of Raf on ERK to promote SC proliferation [41], increase the phosphorylation activity of histone acetyltransferase p300, and enhance the transcriptional activity of Myod to promote SC differentiation [42,43]. IGF-1 typically acts via its receptor to activate the PI3K pathway. For the first time, we demonstrated that FGF21 impairs SC proliferation and differentiation by inhibiting the PI3K/Akt pathway in skeletal muscles, leading to the development of sarcopenia in DC. Interestingly, PI3K/Akt activation also increases the activity of myocyte enhancer factor 2 and promotes fiber-type switching to a slow oxidative phenotype. This is consistent with our results, which showed that the cross-sectional area of type I muscle fibers (Fig. 6I) was significantly enlarged after FGF21 knockdown.

KLB is a single-channel transmembrane receptor that binds to FGFRs as a co-receptor and is responsible for FGF19/21/23 signal transduction [44,45]; FGF21 binds to the FGFR/KLB-a model of the 2:2:1 receptor complex of FGF21:FGFR1:KLB [46]. FGF19/21/23 mainly activates the downstream MAPK, PI3K, PLCγ, and STAT signaling pathways via FGFRS/KLB, and contributes to cell growth, proliferation, differentiation, and apoptosis [47]. KLB is widely distributed in various tissues, with the highest expression noted in fat cells, and in the liver and pancreas. Its expression can also be detected in skeletal muscle [48]. The effect of KLB on muscle wasting may be related to the disease state, and its localization in skeletal muscle is still not fully understood. FGF19 promotes skeletal muscle hypertrophy under physiological conditions via KLB-mediated activation of ERK but does not indicate its site of action. KLB may mediate muscle weakness in patients with chronic obstructive pulmonary disease and co-localize to the plasma membrane and centralized nuclei [49]. In addition to inhibiting mTORC1 activity and reducing myogenic capacity, it has been found to mediate intrauterine growth restriction in a porcine model [50]. In contrast to previous findings, the present study is the first to show that KLB co-localizes with the SC marker Pax7 in a DC mouse model, and that the inhibitory effect of FGF21 on PI3K/Akt is abolished by reducing the expression of PTEN after KLB knockout, resulting in the restoration of SC function without sarcopenia. As a negative regulator of the PI3K-Akt pathway, PTEN also plays an important role in SC homeostasis. A previous study found that PTEN expression in differentiated mature myotubes is low, and high-fat diet feeding or palmitic acid treatment stimulates the expression of PTEN, which impairs muscle cell growth and muscle repair. Skeletal muscle-specific knockout of PTEN promotes muscle regeneration after injury induced by a high-fat diet [51]. KLB activation increased PTEN expression, which was responsible for the inhibition of the PI3K/Akt pathway. However, the mechanism underlying the KLB-mediated regulation of PTEN expression remains unknown and should be explored in future studies.

In summary, we confirmed that the excessive secretion of FGF21 in the liver inhibits SC proliferation and differentiation, leading to skeletal muscle wasting. Hepatocyte-derived FGF21 inhibited the PI3K/Akt pathway in SC via blood circulation and accelerated skeletal muscle loss (Fig. S10). This may explain the strong association between liver dysfunction and sarcopenia in patients with DC, as observed in multiple clinical studies. Most importantly, our results demonstrate restoring normal FGF21 levels by the systemic administration of an FGF21 neutralizing antibody or by reducing KLB expression in skeletal muscle may be a potential new therapeutic strategy for treating DC-related sarcopenia.

Financial Support

This study was supported by the National Natural Science Foundation of China (82170575, 82370900) and Jiangsu Province Key Research and Development Project (BE2022822).

CRediT authorship contribution statement

Da Zhou: Writing – original draft, Formal analysis, Data curation, Conceptualization. **Yifan Shi:** Data curation. **Donghua Zhang:** Investigation. **Junbo Zuo:** Investigation. **Chenghao Zeng:** Investigation.

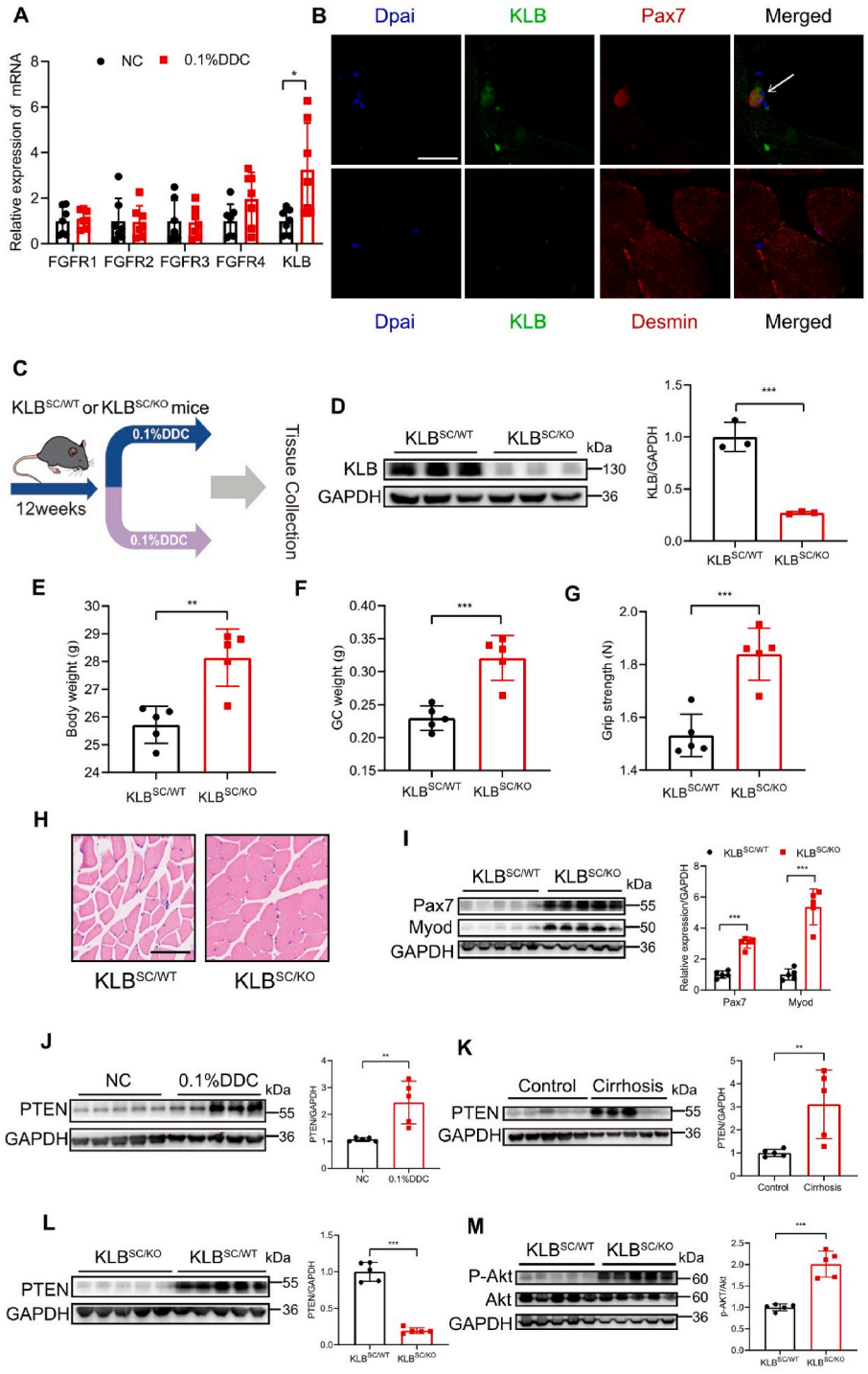

Fig. 8. FGF21 negatively regulates SCs through KLB

(A) Quantitative RT-qPCR of FGFR and KLB expression in GC muscle from NC and 0.1 % DDC mice (n = 7 mice). (B) Representative images of immunofluorescent staining for KLB (green) and Pax7 (red), and KLB (green) and Desmin (red) in GC muscle sections of NC and 0.1 % DDC mice. The nuclei were labeled with DAPI (blue). Scale bars: 25 μm. (C) Experimental scheme. (D) Left panel: Western blot of KLB in $KLB^{SC/WT}$ and $KLB^{SC/KO}$ mice (n = 3 mice). Right panel: Semi-quantitative analysis. (E–G) Body weight, GC muscle weight, and grip strength in $KLB^{SC/WT}$ and $KLB^{SC/KO}$ mice (n = 5 mice). (H) Representative H&E staining images of GC muscle sections from $KLB^{SC/WT}$ and $KLB^{SC/KO}$ mice (n = 3 mice). Scale bars: 100 μm. (I) Western blot and semi-quantitative analysis of Pax7 and Myod expression in $KLB^{SC/WT}$ and $KLB^{SC/KO}$ mice (n = 5 mice). (J) Western blot and semi-quantitative analysis of PTEN in NC and 0.1 % DDC mice (n = 5 mice). (K) Western blot and semi-quantitative analysis of PTEN in control and patients with DC (n = 5 patients). (L) Western blot and semi-quantitative analysis of PTEN in $KLB^{SC/WT}$ and $KLB^{SC/KO}$ mice (n = 5 mice). (M) Western blot and semi-quantitative analysis of *p*-Akt in $KLB^{SC/WT}$ and $KLB^{SC/KO}$ mice (n = 5 mice). Data are shown as mean ± SD. Student's t-test was used to determine statistical significance. *P < 0.05, **P < 0.01, ***P < 0.001. Abbreviations: DDC, 5-diethoxycarbonyl-1,4-dihydrocollidine; GC, gastrocnemius; H&E, hematoxylin and eosin; PTEN, phosphatase and tensin homolog; KLB, klotho beta; FGFR, fibroblast growth factor receptor. (For interpretation of the references to colour in this figure legend, the reader is referred to the Web version of this article.)

Gulsudum Mamtawla: Methodology. **LongChang Huang:** Methodology. **Xuejin Gao:** Supervision. **Li Zhang:** Software. **Xinying Wang:** Writing – review & editing, Conceptualization.

Declaration of competing interest

The authors declare no conflict of interest.

Data availability

Data will be made available on request.

Acknowledgments

We greatly appreciate all of the individuals involved in this study. We also would like to thank Prof Liwei Xie for providing the Pax7-CreER mice.

Appendix A. Supplementary data

Supplementary data to this article can be found online at https://doi.org/10.1016/j.redox.2024.103333.

References

[1] D.Q. Huang, N.A. Terrault, F. Tacke, L.L. Gluud, M. Arrese, E. Bugianesi, R. Loomba, Global epidemiology of cirrhosis - aetiology, trends and predictions, Nat. Rev. Gastroenterol. Hepatol. 20 (2023) 388–398.
[2] X.Y. Xu, H.G. Ding, W.G. Li, J.H. Xu, Y. Han, J.D. Jia, L. Wei, et al., Chinese guidelines on the management of liver cirrhosis (abbreviated version), World J. Gastroenterol. 26 (2020) 7088–7103.
[3] S. Ling, G. Jiang, Q. Que, S. Xu, J. Chen, X. Xu, Liver transplantation in patients with liver failure: twenty years of experience from China, Liver Int. 42 (2022) 2110–2116.
[4] X. Tantai, Y. Liu, Y.H. Yeo, M. Praktiknjo, E. Mauro, Y. Hamaguchi, C. Engelmann, et al., Effect of sarcopenia on survival in patients with cirrhosis: a meta-analysis, J. Hepatol. 76 (2022) 588–599.
[5] M. Kalafateli, K. Mantzoukis, Y. Choi Yau, A.O. Mohammad, S. Arora, S. Rodrigues, M. de Vos, et al., Malnutrition and sarcopenia predict post-liver transplantation outcomes independently of the Model for End-stage Liver Disease score, J Cachexia Sarcopenia Muscle 8 (2017) 113–121.
[6] D. Zhou, D. Zhang, C. Zeng, L. Zhang, X. Gao, X. Wang, Impact of sarcopenia on the survival of patients undergoing liver transplantation for decompensated liver cirrhosis, J Cachexia Sarcopenia Muscle (2023).
[7] S. Dasarathy, M. Merli, Sarcopenia from mechanism to diagnosis and treatment in liver disease, J. Hepatol. 65 (2016) 1232–1244.
[8] C. Tsien, G. Davuluri, D. Singh, A. Allawy, G.A. Ten Have, S. Thapaliya, J. M. Schulze, et al., Metabolic and molecular responses to leucine-enriched branched chain amino acid supplementation in the skeletal muscle of alcoholic cirrhosis, Hepatology 61 (2015) 2018–2029.
[9] S. Reichelt, J. Pratschke, C. Engelmann, U.P. Neumann, G. Lurje, Z. Czigany, Body composition and the skeletal muscle compartment in liver transplantation: turning challenges into opportunities, Am. J. Transplant. 22 (2022) 1943–1957.
[10] R.A. Bhanji, A.J. Montano-Loza, K.D. Watt, Sarcopenia in cirrhosis: looking beyond the skeletal muscle loss to see the systemic disease, Hepatology 70 (2019) 2193–2203.
[11] D. Häussinger, R.K. Dhiman, V. Felipo, B. Görg, R. Jalan, G. Kircheis, M. Merli, et al., Hepatic encephalopathy, Nat. Rev. Dis. Prim. 8 (2022) 43.
[12] E. Solà, P. Ginès, Renal and circulatory dysfunction in cirrhosis: current management and future perspectives, J. Hepatol. 53 (2010) 1135–1145.
[13] H. Yin, F. Price, M.A. Rudnicki, Satellite cells and the muscle stem cell niche, Physiol. Rev. 93 (2013) 23–67.
[14] H. Ding, S. Chen, X. Pan, X. Dai, G. Pan, Z. Li, X. Mai, et al., Transferrin receptor 1 ablation in satellite cells impedes skeletal muscle regeneration through activation of ferroptosis, J Cachexia Sarcopenia Muscle 12 (2021) 746–768.
[15] E.E. Talbert, D.C. Guttridge, Impaired regeneration: a role for the muscle microenvironment in cancer cachexia, Semin. Cell Dev. Biol. 54 (2016) 82–91.
[16] S. Dasarathy, A.J. McCullough, S. Muc, A. Schneyer, C.D. Bennett, M. Dodig, S. C. Kalhan, Sarcopenia associated with portosystemic shunting is reversed by follistatin, J. Hepatol. 54 (2011) 915–921.
[17] C. Degirolamo, C. Sabbà, A. Moschetta, Therapeutic potential of the endocrine fibroblast growth factors FGF19, FGF21 and FGF23, Nat. Rev. Drug Discov. 15 (2016) 51–69.
[18] M. Farooq, A.W. Khan, M.S. Kim, S. Choi, The role of fibroblast growth factor (FGF) signaling in tissue repair and regeneration, Cells 10 (2021).
[19] B. Benoit, E. Meugnier, M. Castelli, S. Chanon, A. Vieille-Marchiset, C. Durand, N. Bendridi, et al., Fibroblast growth factor 19 regulates skeletal muscle mass and ameliorates muscle wasting in mice, Nat. Med. 23 (2017) 990–996.
[20] L. Jin, L. Geng, L. Ying, L. Shu, K. Ye, R. Yang, Y. Liu, et al., FGF21-Sirtuin 3 Axis confers the protective effects of exercise against diabetic cardiomyopathy by governing mitochondrial integrity, Circulation 146 (2022) 1537–1557.
[21] D. Wang, F. Liu, L. Zhu, P. Lin, F. Han, X. Wang, X. Tan, et al., FGF21 alleviates neuroinflammation following ischemic stroke by modulating the temporal and spatial dynamics of microglia/macrophages, J. Neuroinflammation 17 (2020) 257.
[22] L.J. Oost, M. Kustermann, A. Armani, B. Blaauw, V. Romanello, Fibroblast growth factor 21 controls mitophagy and muscle mass, J Cachexia Sarcopenia Muscle 10 (2019) 630–642.
[23] C. Tezze, V. Romanello, M.A. Desbats, G.P. Fadini, M. Albiero, G. Favaro, S. Ciciliot, et al., Age-associated loss of OPA1 in muscle impacts muscle mass, metabolic homeostasis, systemic inflammation, and epithelial senescence, Cell Metabol. 25 (2017) 1374–1389.e1376.
[24] F.R. Ponziani, A. Picca, E. Marzetti, R. Calvani, G. Conta, F. Del Chierico, G. Capuani, et al., Characterization of the gut-liver-muscle axis in cirrhotic patients with sarcopenia, Liver Int. (2021).
[25] B. Pawlikowski, T.O. Vogler, K. Gadek, B.B. Olwin, Regulation of skeletal muscle stem cells by fibroblast growth factors, Dev. Dynam. 246 (2017) 359–367.
[26] M. Ebadi, R.A. Bhanji, V.C. Mazurak, A.J. Montano-Loza, Sarcopenia in cirrhosis: from pathogenesis to interventions, J. Gastroenterol. 54 (2019) 845–859.
[27] W. Vankrunkelsven, S. Thiessen, S. Derde, E. Vervoort, I. Derese, I. Pintelon, H. Matheussen, et al., Development of muscle weakness in a mouse model of critical illness: does fibroblast growth factor 21 play a role? Skeletal Muscle 13 (2023) 12.
[28] T. Nishimura, Y. Nakatake, M. Konishi, N. Itoh, Identification of a novel FGF, FGF-21, preferentially expressed in the liver, Biochim. Biophys. Acta 1492 (2000) 203–206.
[29] A. Mauro, Satellite cell of skeletal muscle fibers, J. Biophys. Biochem. Cytol. 9 (1961) 493–495.
[30] M.N. Wosczyna, T.A. Rando, A muscle stem cell support group: coordinated cellular responses in muscle regeneration, Dev. Cell 46 (2018) 135–143.
[31] B. Evano, S. Khalilian, G. Le Carrou, G. Almouzni, S. Tajbakhsh, Dynamics of asymmetric and symmetric divisions of muscle stem cells in vivo and on artificial niches, Cell Rep. 30 (2020) 3195–3206.e3197.
[32] M.A. Egerman, S.M. Cadena, J.A. Gilbert, A. Meyer, H.N. Nelson, S.E. Swalley, C. Mallozzi, et al., GDF11 increases with age and inhibits skeletal muscle regeneration, Cell Metabol. 22 (2015) 164–174.
[33] M.A. Rudnicki, P.N. Schnegelsberg, R.H. Stead, T. Braun, H.H. Arnold, R. Jaenisch, MyoD or Myf-5 is required for the formation of skeletal muscle, Cell 75 (1993) 1351–1359.
[34] J.M. Venuti, J.H. Morris, J.L. Vivian, E.N. Olson, W.H. Klein, Myogenin is required for late but not early aspects of myogenesis during mouse development, J. Cell Biol. 128 (1995) 563–576.
[35] P. Sousa-Victor, S. Gutarra, L. García-Prat, J. Rodriguez-Ubreva, L. Ortet, V. Ruiz-Bonilla, M. Jardí, et al., Geriatric muscle stem cells switch reversible quiescence into senescence, Nature 506 (2014) 316–321.
[36] F. Huo, Q. Liu, H. Liu, Contribution of muscle satellite cells to sarcopenia, Front. Physiol. 13 (2022) 892749.
[37] J.D. Bernet, J.D. Doles, J.K. Hall, K. Kelly Tanaka, T.A. Carter, B.B. Olwin, p38 MAPK signaling underlies a cell-autonomous loss of stem cell self-renewal in skeletal muscle of aged mice, Nat. Med. 20 (2014) 265–271.
[38] N. Pietrosemoli, S. Mella, S. Yennek, M.B. Baghdadi, H. Sakai, R. Sambasivan, F. Pala, et al., Comparison of multiple transcriptomes exposes unified and divergent features of quiescent and activated skeletal muscle stem cells, Skeletal Muscle 7 (2017) 28.
[39] J.T. Rodgers, K.Y. King, J.O. Brett, M.J. Cromie, G.W. Charville, K.K. Maguire, C. Brunson, et al., mTORC1 controls the adaptive transition of quiescent stem cells from G0 to G(Alert), Nature 510 (2014) 393–396.
[40] J.T. Rodgers, M.D. Schroeder, C. Ma, T.A. Rando, HGFA is an injury-regulated systemic factor that induces the transition of stem cells into G(alert), Cell Rep. 19 (2017) 479–486.
[41] T. Endo, Postnatal skeletal muscle myogenesis governed by signal transduction networks: MAPKs and PI3K-Akt control multiple steps, Biochem. Biophys. Res. Commun. 682 (2023) 223–243.
[42] E.M. Wilson, P. Rotwein, Selective control of skeletal muscle differentiation by Akt1, J. Biol. Chem. 282 (2007) 5106–5110.
[43] C. Serra, D. Palacios, C. Mozzetta, S.V. Forcales, I. Morantte, M. Ripani, D.R. Jones, et al., Functional interdependence at the chromatin level between the MKK6/p38 and IGF1/PI3K/AKT pathways during muscle differentiation, Mol. Cell 28 (2007) 200–213.

[44] Y. Ogawa, H. Kurosu, M. Yamamoto, A. Nandi, K.P. Rosenblatt, R. Goetz, A. V. Eliseenkova, et al., BetaKlotho is required for metabolic activity of fibroblast growth factor 21, Proc. Natl. Acad. Sci. U. S. A. 104 (2007) 7432–7437.
[45] X. Wu, H. Ge, J. Gupte, J. Weiszmann, G. Shimamoto, J. Stevens, N. Hawkins, et al., Co-receptor requirements for fibroblast growth factor-19 signaling, J. Biol. Chem. 282 (2007) 29069–29072.
[46] D.M. Kilkenny, J.V. Rocheleau, The FGF21 receptor signaling complex: klothoβ, FGFR1c, and other regulatory interactions, Vitam. Horm. 101 (2016) 17–58.
[47] D.M. Ornitz, N. Itoh, The fibroblast growth factor signaling pathway, Wiley Interdiscip Rev Dev Biol 4 (2015) 215–266.
[48] K. Fon Tacer, A.L. Bookout, X. Ding, H. Kurosu, G.B. John, L. Wang, R. Goetz, et al., Research resource: comprehensive expression atlas of the fibroblast growth factor system in adult mouse, Mol. Endocrinol. 24 (2010) 2050–2064.
[49] M.S. Patel, A.V. Donaldson, A. Lewis, S.A. Natanek, J.Y. Lee, Y.M. Andersson, G. Haji, et al., Klotho and smoking–An interplay influencing the skeletal muscle function deficits that occur in COPD, Respir. Med. 113 (2016) 50–56.
[50] Y. Cortes-Araya, C. Stenhouse, M. Salavati, S.O. Dan-Jumbo, W. Ho, C.J. Ashworth, E. Clark, et al., KLB dysregulation mediates disrupted muscle development in intrauterine growth restriction, J. Physiol. 600 (2022) 1771–1790.
[51] Z. Hu, H. Wang, I.H. Lee, S. Modi, X. Wang, J. Du, W.E. Mitch, PTEN inhibition improves muscle regeneration in mice fed a high-fat diet, Diabetes 59 (2010) 1312–1320.